Conversion of CO$_2$ in a packed-bed dielectric barrier discharge reactor

Atindra M. Banerjee,[a] Joel Billinger, and Karen J. Nordheden[b]
Department of Chemical and Petroleum Engineering, University of Kansas, 1530 W. 15th Street, Lawrence, Kansas 66045

Floran J. J. Peeters[c]
Dutch Institute for Fundamental Energy Research (DIFFER), P.O. Box 6336, 5600 HH Eindhoven, The Netherlands

The conversion of CO$_2$ into CO and O$_2$ in a quartz cylindrical packed-bed dielectric reactor has been studied using CO$_2$ and Ar gas mixtures at atmospheric pressure and near ambient temperature with quartz wool, γ-Al$_2$O$_3$, and TiO$_2$ packing. The highest energy efficiencies and conversion rates were observed with TiO$_2$ packing in 20% CO$_2$ in Ar: 30% conversion with 2.9% energy efficiency, and 17.5% conversion with 5.0% energy efficiency. Both γ-Al$_2$O$_3$ and quartz wool also showed an enhancement in conversion over an unpacked reactor. The percentage of CO$_2$ to Ar in the range of 20%–60% is shown to have only a minor effect on reactor performance. Conversion as a function of power input and flow rate is studied in detail for γ-Al$_2$O$_3$ and TiO$_2$ packing with similar particle sizes. In both cases, simple chemical kinetic models show that the CO production rate is nearly equal for both materials, while reverse reaction rates to CO$_2$ are doubled for γ-Al$_2$O$_3$ compared to TiO$_2$. From detailed charge–voltage (Q-V) analysis of all four reactor configurations, it is revealed that the electric field at which discharging occurs is higher for both γ-Al$_2$O$_3$ and TiO$_2$ as compared to the empty or quartz wool filled reactors. Comparing kinetic model results with the electrical Q-V analysis, it appears likely that the higher and similar magnitude electric fields occurring with γ-Al$_2$O$_3$ and TiO$_2$ are directly responsible for the increased CO production rates via increased electron energies in the discharge. The higher reverse reaction rates for γ-Al$_2$O$_3$, and its subsequent poorer performance compared to TiO$_2$, can be attributed to a significantly higher effective surface area, which increases undesirable surface reactions between CO and oxygen species. *Published by the AVS.*
https://doi.org/10.1116/1.5024400

I. INTRODUCTION

Various strategies have been proposed to reduce atmospheric levels of the greenhouse gas CO$_2$, including the limitation of emissions, carbon capture and storage, or conversion and utilization. The latter is the most attractive solution since the conversion of CO$_2$ into value-added fuels and chemicals would not only reduce the global levels of CO$_2$, but also our dependence on fossil fuels.[1–3] As an example, the CO obtained from the splitting of CO$_2$ could be combined with H$_2$ to form synthesis gas (syngas) for Fischer–Tropsch production of methanol or other liquid hydrocarbon fuels.[1] However, CO$_2$ is thermodynamically a very stable molecule and considerable energy is required to dissociate it. In order for the utilization of CO$_2$ to be economically viable, an energy efficient conversion process is required.

Direct thermal, thermochemical, electrochemical, or photochemical methods can be utilized for the splitting of CO$_2$.[1] Lebouvier et al.[2] carried out an assessment of various technologies for syngas production by CO$_2$ dissociation and concluded that plasma-based techniques are more efficient by virtue of their compactness, faster reaction times, and lower operational costs as compared to coal gasification and reforming. However, the assessment also indicated that the energy

efficiencies, conversion rates, and mass flow rates have to be improved for the existing plasma processes to be competitive with conventional processes for syngas production.

Plasma reactors offer an attractive alternative to traditional conversion processes since the energetic electrons and active species in the plasma can stimulate dissociation even when the bulk gas is near room temperature and atmospheric pressure.[1–4] The use of packed-bed dielectric barrier discharge (DBD) reactors for CO$_2$ conversion is of significant interest because the presence of packing materials in the plasma can intensify the average electric field and consequently improve the conversion and efficiency of the process.[5–7] Combining packing materials with plasma in this way is commonly referred to as "plasma catalysis," although a thorough understanding of the physical and chemical interactions of the plasma with these materials is lacking.[5] There have been some previous reports of CO$_2$ splitting using various cylindrical DBD plasma configurations.[6–10] Yu et al.[8] studied the effects of silica gel, quartz, α-Al$_2$O$_3$, γ-Al$_2$O$_3$, and CaTiO$_3$ dielectric pellets for packing materials. With a discharge length of 7.5 cm and discharge gap of 4 mm, they achieved a maximum CO$_2$ conversion of 16% using CaTiO$_3$ pellets at a power of ~35 W and flow rate of 40 sccm. Mei et al.[9] have found that the addition of BaTiO$_3$ packing significantly enhances the electric field and mean electron energy of the discharge. The addition of glass beads or BaTiO$_3$ packing both resulted in increased CO$_2$ conversions over that of the unpacked reactor. With a discharge length of

[a]Present address: Bhabha Atomic Research Centre (BARC), Mumbai-400085, India.
[b]Electronic mail: nordhed@ku.edu
[c]Electronic mail: F.J.J.Peeters@differ.nl

6 cm, a gap of 3 mm containing $BaTiO_3$ packing, a flow rate of 50 sccm, and a discharge power of 40 W, they achieved a maximum conversion of ~23%. Recently, Tu et al.[11] have shown that the addition of TiO_2 particles to a nitrogen DBD produced a shift in the electron energy distribution toward higher energy electrons.

In this work, the conversion of CO_2 is investigated in a packed-bed dielectric barrier discharge reactor with quartz wool, γ-Al_2O_3, and TiO_2 packing materials with the aim of determining the relative contributions of plasma and packing to the conversion process. To this end, the conversion is studied as a function of power and flow rate to obtain simplified kinetic rates, while the plasma is studied using charge– voltage (Q-V) analysis to obtain the electric field strengths at which discharging occurs. By combining these two approaches, the effect of packing on the plasma and the differences in plasma chemical interactions with the packing material surfaces are assessed.

II. EXPERIMENT

The experiments were conducted in a cylindrical packed-bed DBD reactor as shown in Fig. 1. The DBD reactor consisted of two coaxial quartz tubes. The outer tube was 0.75 in. outer diameter (OD) and 0.55 in. inner diameter (ID). The inner tube was 0.25 in. OD, resulting in an annular gap of 0.15 in. (or about 3.8 mm). The high voltage electrode was a 1/8 in. stainless steel rod placed within the inner tube, and the grounded electrode was a stainless steel mesh wrapped around the outer tube. The length of the mesh defined the discharge length which was kept fixed at 2.5 cm, resulting in an unpacked reactor volume of about $3.0\,cm^3$. The annular zone between the two tubes was filled with the dielectric packing material (extending ~2 mm on either end of the grounded mesh) that was held in place with quartz wool. The γ-Al_2O_3 (Sigma Aldrich) and the TiO_2 (Aerolyst, Degussa) powders were first dry pressed and then sieved through 20–40 mesh, resulting in irregularly shaped granular

particle sizes ranging from 420 to 840 μm in diameter. Surface analysis of the packing materials was conducted using a Quantachrome NOVA 2000e N_2-Brunauer-Emmett-Teller (BET) sorption analyzer, while void fractions were measured by water displacement.

A high voltage AC power supply (PVM500) operated at 27–30 kHz was used to generate the plasma. The applied voltage and frequency were measured with a high voltage probe (Tektronix P6015A) and the voltage on an external capacitor (285 pF) placed in series between the outer mesh electrode and ground, was measured to obtain the charge generated in the discharge. All signals were recorded on a digital oscilloscope (Agilent DSO6104A), and the power supplied to the reactor was calculated from the area of the Q-V Lissajous figures.[12]

The feed gases were controlled by mass flow controllers and entered the reactor through an electrically isolated tee. The total effluent flow rate was also monitored using an Agilent ADM2000 flowmeter. Temperature in the discharge zone was measured with an optical pyrometer. Prior to conversion measurements, an argon plasma was run to minimize adsorbed water vapor and impurities. Products of reaction were evaluated for CO_2 decomposition using an online SRI Instruments gas-chromatograph (GC) fitted with both a thermal conductivity detector and a methanizer-equipped flame ionization detector. All experiments were conducted at atmospheric pressure, and all conversion measurements were taken at steady-state. CO_2 conversions were measured from the CO_2 concentration at the inlet and outlet of the reactor and the CO and O_2 yields were measured at the outlet of the reactor. The CO_2 conversion, energy efficiency and specific energy input (SEI) are defined as

$$CO_2 \text{ conversion } (\%) = \frac{CO_2 \text{ (inlet)} - CO_2 \text{ (outlet)}}{CO_2 \text{ (inlet)}} \times 100,$$

(1)

$$\text{Energy Efficiency}(\%)$$
$$= \frac{CO_2 \text{ converted (mol s}^{-1}) \times \Delta H \text{ (J mol}^{-1})}{\text{Power(W)}} \times 100,$$

(2)

$$\text{SEI}\left(\frac{eV}{\text{molecule}}\right) = \frac{\text{Power (W)}}{\text{Total flow (sccm)}} \times 13.8,$$

(3)

where $\Delta H = 279.8$ kJ/mole or 2.9 eV/molecule at 300 K and 1 atm. In Eq. (3), the total flow is the sum of Ar and CO_2 flows at the inlet, and the constant term represents unit conversions assuming the flows are in units of sccm, defined at 273.15 K and 1 atm.

III. THEORY AND MODELING

A. Kinetics of the CO₂ conversion

In order to understand the effect of residence time on the conversion of CO_2, a simplified reaction model is developed assuming both the conversion of CO_2 (forward reaction) and the recombination of CO (reverse reaction) are first-order reactions. The model assumes constant volume (V), constant
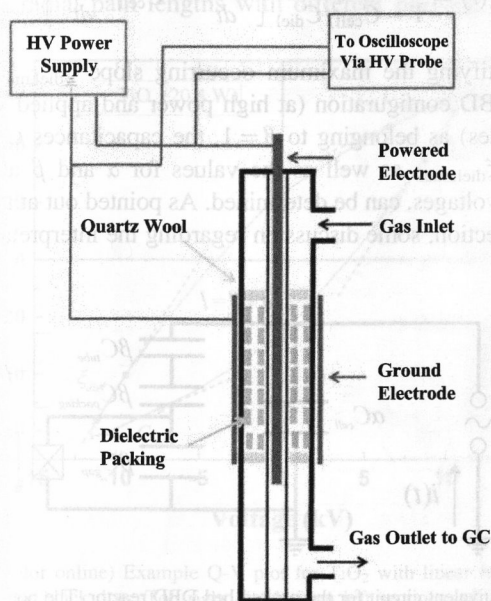

HV Power Supply

To Oscilloscope Via HV Probe

Powered Electrode

Gas Inlet

Quartz Wool

Ground Electrode

Dielectric Packing

Gas Outlet to GC

FIG. 1. (Color online) Schematic diagram of the experimental setup.

temperature, and that residence time, t_{res}, in seconds, is given by

$$t_{res}\,(s) = \frac{(\text{Void fraction}) \times V\,(cm^3)}{\text{Total flow (sccm)}} \times 60. \qquad (4)$$

The material balances for CO_2 and CO are given by

$$\frac{d[CO_2]}{dt} = -\frac{d[CO]}{dt} = -k_f[CO_2] + k_r[CO], \qquad (5)$$

where the reaction rate constants for forward reactions, k_f, and reverse reactions, k_r, both have units of s^{-1}. Furthermore it is assumed the sum of the CO and CO_2 densities must be equal to the original CO_2 inlet density

$$[CO] + [CO_2] = [CO_2]_{inlet}. \qquad (6)$$

Solving these for the fraction of CO_2 converted as a function of residence time gives

$$\frac{[CO_2]_{inlet} - [CO_2]}{[CO_2]_{inlet}} = \frac{k_f}{k_f + k_r}\left[1 - e^{-(k_f + k_r)t_{res}}\right]. \qquad (7)$$

The assumption of first-order reverse reactions for CO is checked against a second-order reverse reaction model with material balances

$$\frac{d[CO_2]}{dt} = -\frac{d[CO]}{dt} = -k_f[CO_2] + \frac{k_r}{[CO_2]_{inlet}}[CO]^2, \qquad (8)$$

where the units of k_r are once again in s^{-1} by normalizing the rate constant against the initial CO_2 density. For the second order model it should be pointed out that $k_r[CO]^2$ is actually $k_r[CO][O]$, with $[O]$ assumed to be proportional to $[CO]$. Equation (8) is solved and fitted to the data numerically, but otherwise treated in the same way as the first order model.

B. Charge-voltage analysis

The experimental Q-V data are analyzed using the model of partial discharging in DBDs by Peeters and Van de Sanden.[13] This model takes into account that plasma discharges may cover only part of the available surface area during a single voltage half-cycle, thus allowing for a more accurate comparison of discharges ignited at different applied voltage amplitudes. The original model was intended for planar DBD geometries with parallelogram Q-V plots, although it has also been applied to cylindrical packed bed DBD geometries.[10,14] The interpretation of this model for the current geometry is discussed after the model is introduced. The main goal behind the analysis in this section is to estimate the electric field strength $E_{discharge}$ at which discharging occurs for each packing material. In the electrical model, each material is assigned its own capacitance: C_{tube} is the dielectric capacitance provided by the quartz tubes (inner and outer), $C_{packing}$ the effective series capacitance of the packing material and C_{gap} the capacitance of the gas gap. While the actual geometry of a packed bed reactor consists

of multiple gas gaps and capacitive pellets, our interest is in the overall radial voltage drop across the gas, allowing for the bunching together of all the various gas gaps in a single component. Though C_{tube} is a constant throughout this study, $C_{packing}$ and C_{gap} will depend on the packing. All of these capacitances in series determine the cell capacitance C_{cell}, with C_{tube} and $C_{packing}$ in series forming the full dielectric capacitance C_{diel}

$$\frac{1}{C_{cell}} = \frac{1}{C_{tube}} + \frac{1}{C_{packing}} + \frac{1}{C_{gap}} = \frac{1}{C_{diel}} + \frac{1}{C_{gap}}. \qquad (9)$$

To account for partial discharging, all of these capacitances are split into a nondischarging fraction α and a discharging fraction β, with $\alpha + \beta = 1$, such that the equivalent circuit of the packed bed reactor appears as depicted in Fig. 2. Note that α and β are not time-dependent and are assigned a constant value for each Q-V plot.

As discussed by Peeters and van den Sanden,[13] the lower slopes in Q-V plots can be identified as the full cell capacitance C_{cell}, while the steepest slopes, termed ξ_{diel}, will depend on α and β as

$$\zeta_{diel} = \alpha C_{cell} + \beta C_{diel}. \qquad (10)$$

Provided C_{cell}, C_{diel} and $\beta = \alpha - 1$ are assigned values, the gap voltage over time $U_{gap}(t)$ for each Q-V plot can be calculated using

$$U_{gap}(t) = \left(1 + \frac{\alpha}{\beta}\frac{C_{cell}}{C_{diel}}\right)V(t) - \frac{1}{\beta C_{diel}}Q(t), \qquad (11)$$

with $V(t)$ the applied voltage and $Q(t)$ the measured charge in the Q-V plot, derived by integrating the current $I(t)$ on a measurement capacitor. The plasma current, $i_{plasma}(t)$, does not depend on α and β and is calculated using

$$i_{plasma}(t) = \frac{1}{1 - C_{cell}/C_{diel}}\left[\frac{dQ(t)}{dt} - C_{cell}\frac{dV(t)}{dt}\right]. \qquad (12)$$

By identifying the maximum occurring slope $\xi_{diel,max}$ for a given DBD configuration (at high power and applied voltage amplitudes) as belonging to $\beta = 1$, the capacitances C_{cell} and $C_{diel} = \xi_{diel,max}$, as well as the values for α and β at lower applied voltages, can be determined. As pointed out at the start of this section, some discussion regarding the interpretation of
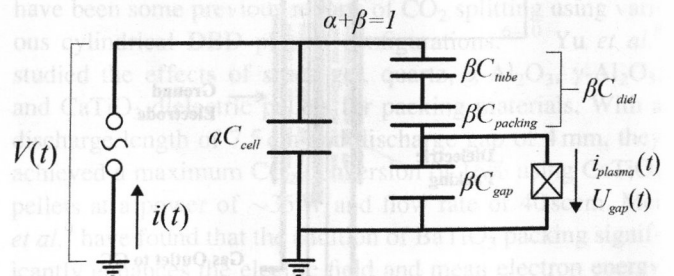

FIG. 2. Equivalent circuit for the packed bed DBD reactor. The nondischarging fraction αC_{cell} contains all nondischarging capacitances αC_{tube}, $\alpha C_{packing}$, and αC_{gap} in series. Plasma is only formed parallel to βC_{gap}.

this model for the ellipsoidlike Q-V plots is desirable. Figure 3 depicts a worst-case Q-V plot for TiO_2 packing. Starting at the bottom left corner, a gradual increase in slope from C_{cell} to some higher value, which we identify here as ξ_{diel}, occurs. With C_{cell} and C_{diel} being constants for a given geometry, a more accurate model would include a time-dependent ξ_{diel} in Eq. (10), with α decreasing and β increasing as the voltage half-cycle progresses. The increasing β would then represent discharges growing perpendicularly to the radial direction in the packed bed until the maximum surface coverage for that applied voltage amplitude is reached. A model taking this into account would more accurately reflect the gap voltage $U_{gap}(t)$ in the area exposed to discharges at each instant. Instead, we greatly simplify matters by assigning a constant β with a constant ξ_{diel} to any given discharge, which represents the maximum extent of the discharges achieved during a half-cycle. This means we only accurately determine $U_{gap}(t)$ near the end of each discharge half-cycle, where for earlier points in time it is an area-averaged gap voltage, as it occurs within the area defined by β.

Figure 3 illustrates how C_{cell} and ξ_{diel} are determined: the rounded edges in the bottom left and top right corners are disregarded, as these are artifacts resulting from the averaging of the $Q(t)$ and $V(t)$ over 30 cycles. From there, a maximum range over which the slope on either side of the corner point is constant is manually determined. Linear fits within these ranges provide the slopes and fitting errors, with the additional constraint that the slopes in either half-cycle are equal.

The maximum $U_{gap}(t)$ occurring near the end of a discharge half-cycle is identified as the "burning voltage" U_b of the discharge.[13] The burning voltage is essentially the breakdown voltage of the discharge, but specific to the repeating discharges occurring in a continuously operating DBD. Comparing U_b outright between different packing materials is not very instructive, since there is also a significant difference in radial path lengths with different packing. Instead,
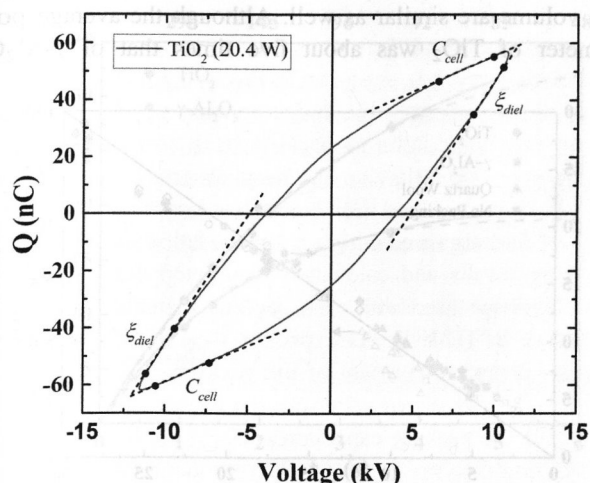
the (average) radial electric field $E_{discharge}$ in the gas is determined via

$$E_{discharge} = \frac{U_b}{f \times d_{gap,unpacked}}, \qquad (13)$$

where f is the electrical void fraction of the packing material and $d_{gap,unpacked}$ is the radial gap width between the inner and outer quartz tube in the unpacked reactor. The electrical void fraction f due to the various packing materials is calculated from the ratio of gap capacitances C_{gap} between unpacked and packed reactors

$$f = \frac{C_{gap,unpacked}}{C_{gap,packed}} = \frac{d_{gap,packed}}{d_{gap,unpacked}}. \qquad (14)$$

The capacitances $C_{gap,unpacked}$ and $C_{gap,packed}$ are calculated using Eq. (9), where both C_{cell} and $C_{diel} = \xi_{diel,max}$ are taken from the Q-V analysis at the highest applied voltage amplitude. The last equality in Eq. (14) assumes a planar gap, where the packing consists of a single slab, or slabs, with uniform thickness. With the actual geometry consisting of a cylindrical capacitor randomly filled with low and high permittivity material in the form of gas and packing, an estimate of the validity of Eq. (14) is desirable. For the unpacked reactor, the elementary equations for a planar capacitor and the more realistic coaxial capacitor reveals that $C_{gap,unpacked}$ is overestimated by no more than 13% for the geometry in this study. As the available gap space is filled with packing, which can be approximated by a series of thin coaxial shells with alternating low and high permittivity, individual low permittivity shells can be more accurately approximated by planar capacitors than is the case for the unpacked reactor. Hence, the last equality in Eq. (14) is accurate to within 13%.

IV. RESULTS AND DISCUSSION

A. CO₂ conversion

The conversion of CO_2 and energy efficiency as a function of power, for a 20% CO_2 in argon mixture and a total flow of 35 sccm, with the various packing materials as a parameter are shown in Figs. 4(a) and 4(b), respectively. For comparison, the conversion in the unpacked DBD reactor is also shown. For all cases, the CO_2 conversion increases with increasing power and the presence of packing results in overall higher conversion rates. The reactor temperature varied from 50 to 70 °C for the range of conditions studied.

The highest conversion is observed for TiO_2 packing at 30% (with 2.9% energy efficiency), and the highest energy efficiency observed, also for TiO_2, is ~5.0% (with 17.5% conversion). At the highest conversion, ~2.0 sccm of CO can be produced from 7 sccm of CO_2 inlet flow at a power of 15 W. Both γ-Al_2O_3 and quartz wool also show an enhancement in conversion and efficiency over an unpacked reactor. Adding surface area to the reactor leads to improved conversion and energy efficiency. This is despite the packing likely resulting in increased gas flow velocity at constant mass flow and a subsequent reduction of average residence time in the reactor.
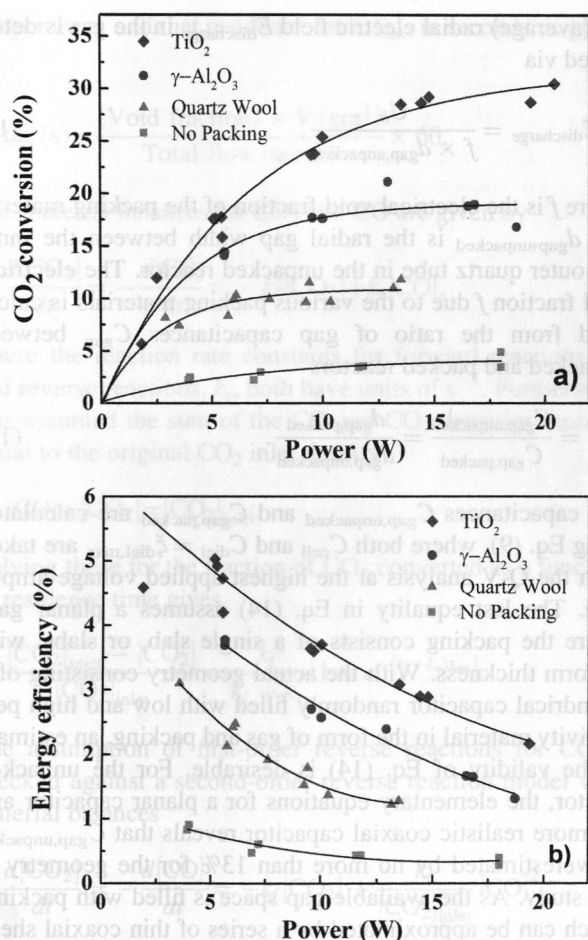

FIG. 3. (Color online) Example Q-V plot for TiO_2 with linear fit intervals indicated by black dots. Top right and bottom left sections are fitted with equal slopes for C_{cell} and ξ_{diel} with equal fit intervals. TiO_2 shows the strongest deviation from ideal parallelogram Q-V plots.

FIG. 4. (Color online) (a) CO$_2$ conversion and (b) energy efficiency as a function of power with dielectric packing a parameter (20% CO$_2$ in argon, 35 sccm total flow). The lines are guides to the eye.

For all packing materials, the highest energy efficiency occurs at low power and then decreases with increasing power. The TiO$_2$ and γ-Al$_2$O$_3$ packing materials have higher energy efficiencies compared with the quartz wool and no packing. From Fig. 4(a), the lowest CO$_2$ conversion occurs at low power and then increases with increasing power. The end result is that the higher conversion rates correspond to lower energy efficiencies. The reduction in energy efficiency can, in part, be explained by the increase in conversion: as the concentration of CO in the reactor increases, the number of reverse reactions to CO$_2$ will increase. Since the rate of reverse reactions is at least proportional to the CO concentration, energy loss through reverse reactions can increase significantly with CO concentration. Taking TiO$_2$ as an example, a factor 1.7 increase in conversion is observed between 5 and 20 W, while the efficiency is reduced by a factor 3 over the same range. It is worth noting that reverse reactions of CO are unlikely to occur in the gas-phase at temperatures of 50 to 70 °C in the absence of atomic O, due to high activation energy for reactions with O$_2$ on the order of 1.32 eV.[15] Atomic O will be scarce, since its recombination to O$_2$ is fast and barrierless.[15] Any reverse reactions for CO are likely mediated by the surface of both quartz tube and dielectric packing.

For a 20% CO$_2$ in argon mixture (14.4 W, 35 sccm total flow rate) using TiO$_2$ packing a 28.6% conversion of CO$_2$ corresponds to measured yields of 26.1% CO and 12.8% O$_2$. Within experimental error, this indicates that the conversion is specific only to the desired CO and O$_2$ reaction products. This was true for all packing materials studied as can be seen from the linear relationship of CO and O$_2$ yields versus CO$_2$ conversion shown in Fig. 5. The lines represent the stoichiometric relationships. No other products were observed in the GC and there was no visible coking. These results indicate that the simplified kinetic models introduced in Sec. III should provide an adequate description of the reaction pathways.

Addition of packing to a DBD has previously been shown to increase CO$_2$ conversion and energy efficiency at constant energy input,[16] though the opposite has also been observed.[17] There has been some indication that the dielectric constant of the packing material directly influences the physical characteristics of the discharge and consequently plays a key role in the conversion, but that role is not fully understood.[8–10] It is interesting to note, as shown in Table I, that the dielectric constants are approximately 3.8 for quartz, 10 for alumina, and 86 for TiO$_2$,[18] which indicates that our work agrees with the previously observed trend of enhanced conversion with increasing dielectric constant of the packing material.[8] This effect does not scale linearly, since the increase in conversion for the TiO$_2$ packing is not 8.6 times that of γ-Al$_2$O$_3$. In the section on Q-V analysis the possible direct influence of dielectric constant on reactor performance will be explored further.

The particle size for both packing materials was the same (between 420 and 840 μm in diameter), and the measured void fraction for both γ-Al$_2$O$_3$ and TiO$_2$ packing materials was ~0.70. Surface analysis with BET indicated that the pore volumes per unit mass of the particles were not significantly different, and since their bulk densities are similar [3.97 g/cm^3 for γ-Al$_2$O$_3$ and between 3.84 (anatase) and 4.26 g/cm^3 (rutile) for TiO$_2$],[19] their particle porosities per unit volume are similar as well. Although the average pore diameter of TiO$_2$ was about five times that of γ-Al$_2$O$_3$
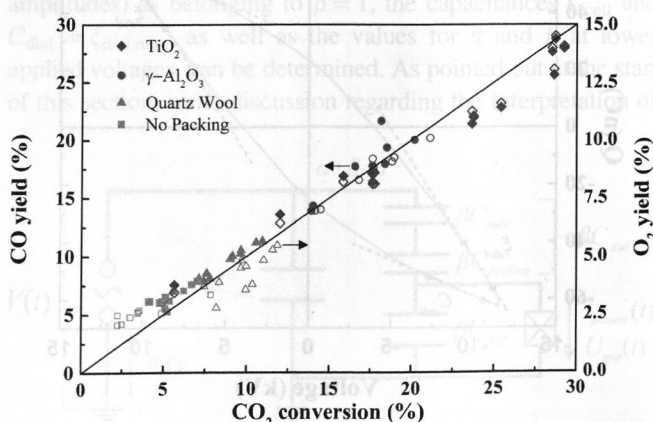

FIG. 5. (Color online) Percent CO yield (closed symbols, left ordinate) and O$_2$ yield (open symbols, right ordinate) as a function of CO$_2$ conversion with dielectric packing a parameter (20% CO$_2$ in argon, 35 sccm total flow).

TABLE I. Physical properties of the dielectric packing materials. –, not applicable.

Dielectric material	BET surface area (m^2/g)	Pore diameter (nm)	Pore volume (cm^3/g)	Dielectric constant, ε_r	Void fraction
Quartz wool	–	–		3.8	–
γ-Al$_2$O$_3$ (Sigma Aldrich)	286	5.54	0.40	10	0.7
TiO$_2$ (Aerolyst, Degussa)	47	29.8	0.35	86	0.7

(5.54 nm vs 29.8 nm), both pore diameters are smaller than the mean-free-paths of both gas particles (order 100 nm) and electrons (order 1 μm), making it unlikely that any charged species can accelerate significantly in the electric fields present within the pores. Plasma, therefore, cannot form or propagate within the pores, minimizing any plasma–surface interaction occurring there.[20] The most significant difference between the two materials is that γ-Al$_2$O$_3$ has six times the BET surface area compared to TiO$_2$, which may affect recombination processes.

The studies of CO$_2$ conversion as a function of total flow rate and feed composition were limited to the TiO$_2$ and γ-Al$_2$O$_3$ packing materials. Figure 6 shows the CO$_2$ conversion as a function of residence time for a 20% CO$_2$ in argon mixture and an input power of 10.8 W. By curve fitting the experimental results with respect to the analytical kinetic model for CO$_2$ conversion given in Eq. (7), the forward and reverse reaction rate constants for the case of γ-Al$_2$O$_3$ packing are estimated to be $k_f = 0.114$ s^{-1}, and $k_r = 0.438$ s^{-1}. In contrast, the forward and reverse reaction rate constants for the case of TiO$_2$ packing are $k_f = 0.126$ s^{-1}, and $k_r = 0.189$ s^{-1}. Comparing this against the model [Eq. (8)] with second order reverse reactions (dashed lines in Fig. 6), a similar trend in the reverse reaction rates are obtained with $k_f = 0.094$ s^{-1}, and $k_r = 2.12$ s^{-1} for γ-Al$_2$O$_3$ and $k_f = 0.115$ s^{-1}, and $k_r = 0.664$ s^{-1} for TiO$_2$. In either model, the forward rates are very similar for γ-Al$_2$O$_3$ and TiO$_2$, while the reverse reaction rate constant for γ-Al$_2$O$_3$ is more than two times that of TiO$_2$. This indicates that the recombination of CO
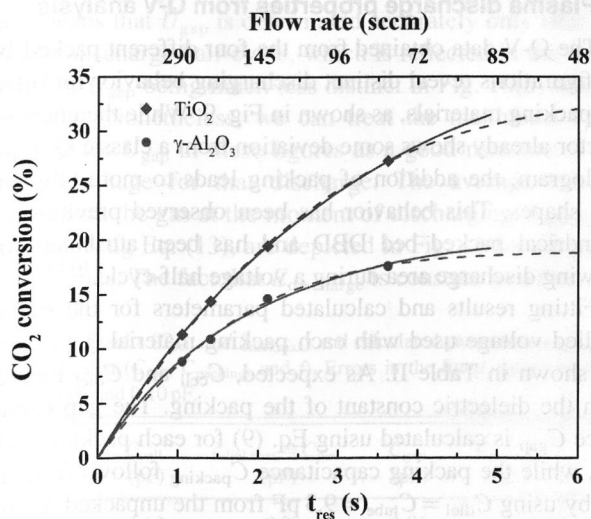
back to CO$_2$ is largely responsible for the overall lower conversion with the γ-Al$_2$O$_3$ packing. With both models fitting the available data equally well, no conclusions can be drawn on whether the reverse reactions to CO$_2$ are best described as first or second order processes.

The effect of total flow rate is compared to the effect of power on the CO$_2$ conversion and energy efficiency in Fig. 7 for TiO$_2$ and γ-Al$_2$O$_3$ packing materials, by plotting both as a function of SEI. Total flow rate and power are varied between 35 and 120 sccm, and between 2.5 and 20 W, respectively. Within the measurement accuracy, there is no distinction between changing power or changing flow. This implies, given that residence time decreases with increasing flow, that "contact time" with the available surface is not a
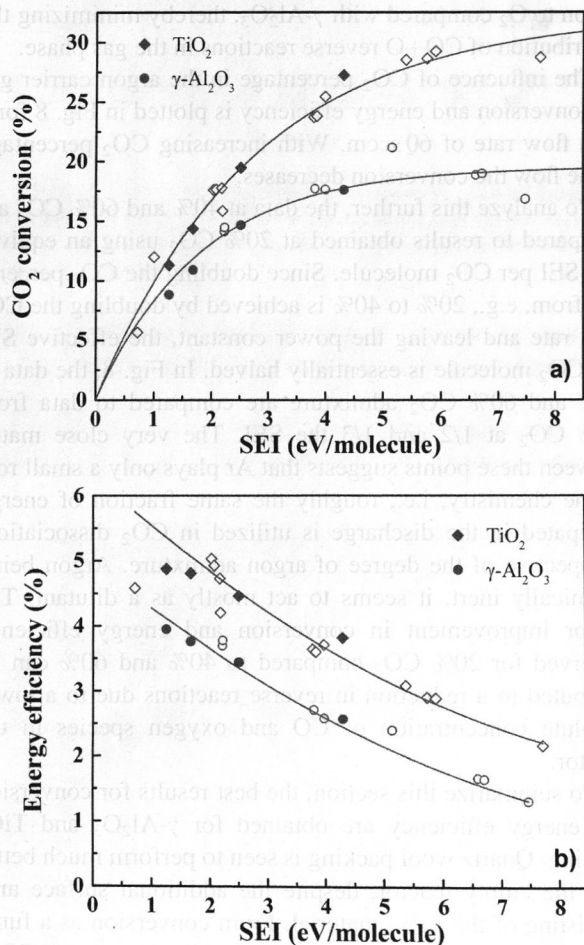
FIG. 7. (Color online) (a) CO$_2$ conversion and (b) energy efficiency as a function of SEI with TiO$_2$ and γ-Al$_2$O$_3$ packing. Closed symbols for a flow rate series between 35 and 120 sccm (20% CO$_2$ in argon, 10.8 ± 0.8 W), open symbols for a power series between 2.5 and 20 W (20% CO$_2$ in argon, 35 sccm).

FIG. 6. (Color online) Effect of residence time on CO$_2$ conversion with TiO$_2$ and γ-Al$_2$O$_3$ packing (20% CO$_2$ in argon, 10.8 ± 0.8 W). The solid lines and dashed lines are curve fits of kinetic models with first order and second order reverse reactions, respectively.

limiting factor in achieving a particular conversion. The conversion is entirely determined by the energy input. Of course, residence times are on the order of several seconds for the flow rates considered here, allowing each gas particle to interact with the surface several thousand times before leaving the reactor.

As already observed in Fig. 6, the initial increase in CO_2 conversion at low SEI (low power or short residence time) is very similar for TiO_2 and γ-Al_2O_3. The major difference between the two packing materials is the magnitude of the eventual saturation of CO_2 conversion, which is nearly double for TiO_2 compared to γ-Al_2O_3. Since the CO production rates are similar, this difference can be attributed to the rate at which reverse reactions from CO to CO_2 take place, which is significantly higher for γ-Al_2O_3 than TiO_2. The factor $\sim$2 difference in CO_2 conversion at high SEI matches with the factor of 2 difference in reverse reaction rates and the six times higher BET surface area for γ-Al_2O_3, supporting the idea that (1) reverse reactions take place mostly on the surface and (2) that γ-Al_2O_3 is more effective at recombining CO with oxygen species. Based on the statement made previously that CO is unlikely to react with O_2 in the gas-phase, another possibility is that TiO_2 enhances atomic O recombination to O_2 compared with γ-Al_2O_3, thereby minimizing the contribution of CO+O reverse reactions in the gas phase.

The influence of CO_2 percentage in the argon carrier gas on conversion and energy efficiency is plotted in Fig. 8 for a total flow rate of 60 sccm. With increasing CO_2 percentage in the flow the conversion decreases.

To analyze this further, the data at 40% and 60% CO_2 are compared to results obtained at 20% CO_2 using an equivalent SEI per CO_2 molecule. Since doubling the CO_2 percentage from, e.g., 20% to 40% is achieved by doubling the CO_2 flow rate and leaving the power constant, the effective SEI per CO_2 molecule is essentially halved. In Fig. 8, the data at 40% and 60% CO_2 admixture are compared to data from 20% CO_2 at 1/2 and 1/3 the SEI. The very close match between these points suggests that Ar plays only a small role in the chemistry, i.e., roughly the same fraction of energy dissipated in the discharge is utilized in CO_2 dissociation, irrespective of the degree of argon admixture. Argon being chemically inert, it seems to act mostly as a dilutant. The minor improvement in conversion and energy efficiency observed for 20% CO_2 compared to 40% and 60% can be attributed to a reduction in reverse reactions due to a lower absolute concentration of CO and oxygen species in the reactor.

To summarize this section, the best results for conversion and energy efficiency are obtained for γ-Al_2O_3 and TiO_2 packing. Quartz wool packing is seen to perform much better than the empty reactor, despite the additional surface area consisting of the same material. From conversion as a function of SEI, it is concluded that the production rate of CO is similar for both packings, while the lower conversion for γ-Al_2O_3 is attributed to increased reverse reactions for this material. The contribution of Ar to the CO_2 dissociation process is relatively small. In Sec. IV B, the effect of the
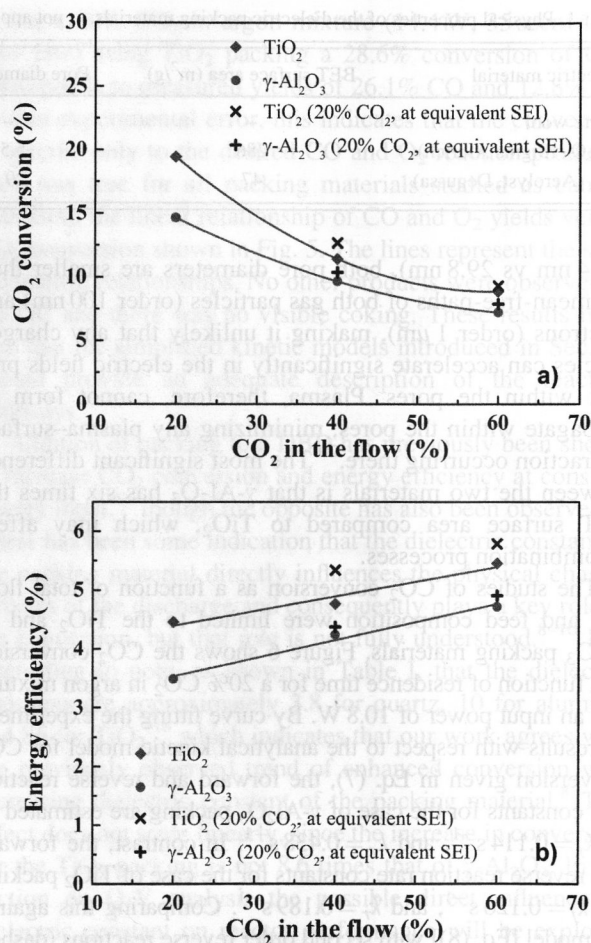

FIG. 8. (Color online) Effect of percent CO_2 in the flow on (a) CO_2 conversion and (b) energy efficiency with TiO_2 and γ-Al_2O_3 packing (60 sccm total flow, 11.4 ± 0.6 W).

packing material on the behavior of the discharge will be investigated using the Q-V analysis.

B. Plasma discharge properties from Q-V analysis

The Q-V data obtained from the four different packed bed configurations reveal distinct discharging behavior for different packing materials, as shown in Fig. 9. While the unpacked reactor already shows some deviation from a classic Q-V parallelogram, the addition of packing leads to more ellipsoid-like shapes. This behavior has been observed previously in cylindrical packed bed DBD and has been attributed to a growing discharge area during a voltage half-cycle.[10,14,21]

Fitting results and calculated parameters for the highest applied voltage used with each packing material (i.e., $\beta = 1$) are shown in Table II. As expected, C_{cell} and C_{diel} increase with the dielectric constant of the packing. The gap capacitance C_{gap} is calculated using Eq. (9) for each packing material, while the packing capacitance $C_{packing}$ follows from Eq. (9) by using $C_{diel} = C_{tube} = 9.3$ pF from the unpacked geometry. The ratio of capacitances of the γ-Al_2O_3 and TiO_2 packing, which have the same particle sizes, are consistent with the ratio of their dielectric constants, and the capacitance of quartz wool is significantly lower than either. The last column
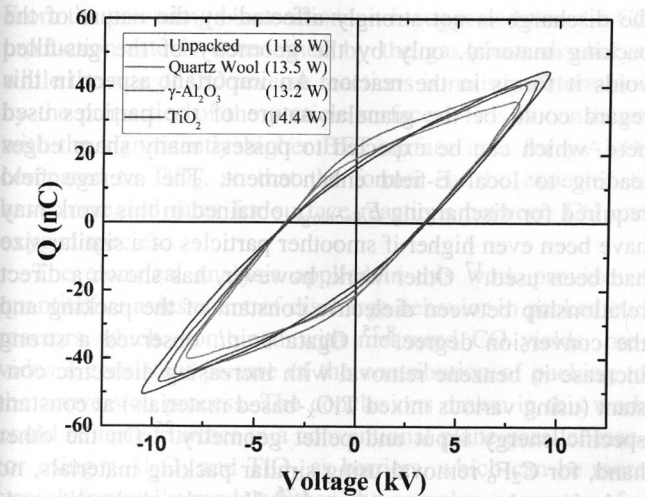
FIG. 9. (Color online) Q-V plots averaged over 30 cycles for all four configurations at similar dissipated powers. With increasing dielectric constant of the packing material the Q-V plots become more ellipsoid-like, with a smoother transition between nondischarging and discharging slopes.

of Table II shows the electrical void fraction, f, via Eq. (14). As discussed in Sec. III, the calculated values of f likely underestimate the true, geometric ratio of $d_{gap,packed}/d_{gap,un-packed}$. This is consistent with the measured void fractions of ~0.7 for γ-Al₂O₃ and TiO₂, versus ~0.5 in Table II. The values of f are, however, the effective electrical void fraction in the equivalent circuit of Fig. 2.

The voltage drop across the gas gaps (excluding the voltage drop across the packing material), $U_{gap}(t)$, and the plasma current, $i_{plasma}(t)$, were obtained from the data using Eqs. (11) and (12), with results depicted in Figs. 10(a) and 10(b) for the extreme cases of unpacked and TiO₂ packed discharges, respectively. In both cases, as plasma current begins to flow, the sign of U_{gap} changes. After some time, U_{gap} levels off at some maximum value, which corresponds to the burning voltage U_b of the discharge.[13] As discussed in Sec. III, applying the model of Fig. 2 to ellipsoid-like Q-V plots means that U_{gap} is determined accurately only near the end of a discharge half-cycle, which is reflected in the leveling off of U_{gap} being much less distinct in Fig. 10(b) than in Fig. 10(a). Nonetheless, we can treat the maximum value observed for U_{gap} in these figures as a good measure of the burning voltage for that discharge. The average electric fields across the gas at the moment of discharging, $E_{discharge}$, obtained using Eq. (13), are depicted in Fig. 11 for all packing materials. The fact that $E_{discharge}$ is constant as a function

TABLE II. Fit results (C_{cell} and $\xi_{diel,max}$) and calculated parameters explained in the main text (C_{gap}, $C_{packing}$, and f). Errors in the fitted capacitance are between 0.05 and 0.10 pF.

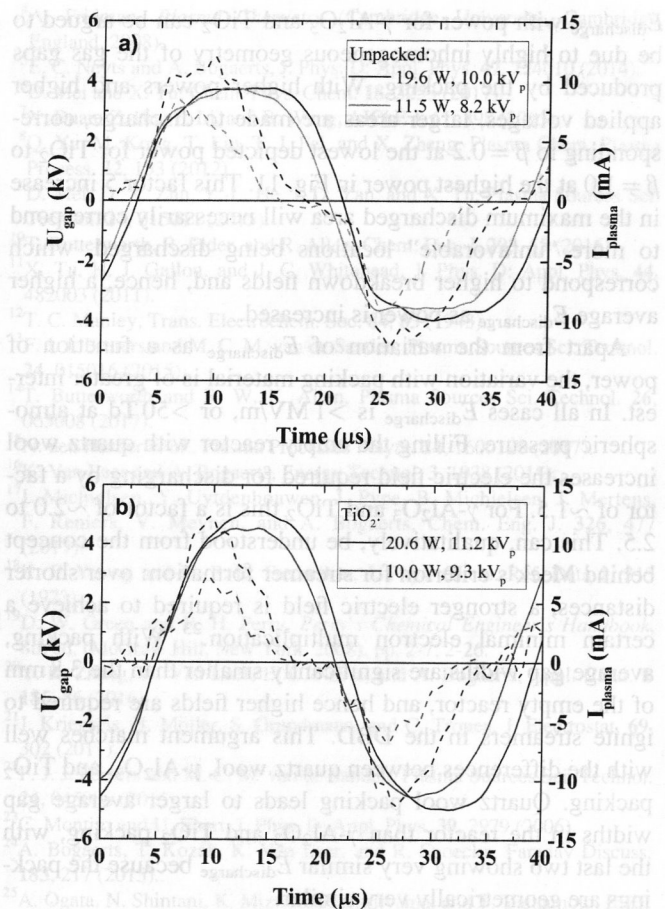| Dielectric material	C_{cell} (pF)	$\xi_{diel,max} = C_{diel}$ (pF)	C_{gap} (pF)	$C_{packing}$ (pF)	f
No packing	1.62	9.3	1.96	—	1
Quartz wool	1.99	8.5	2.60	94	0.75
γ-Al₂O₃	2.62	9.2	3.66	856	0.54
TiO₂	2.67	9.29	3.74	8640	0.52

FIG. 10. (Color online) Area-averaged gap voltages U_{gap} (solid lines) and total plasma current I_{plasma} (dashed lines) over time for (a) the unpacked DBD and (b) TiO₂ packing. The legends indicate dissipated power and the applied voltage amplitude.

of power for both the unpacked reactors and quartz wool is a result of correcting for the maximum discharged areal fraction β.

A constant electric field during discharging was also observed for N₂ in a planar DBD.[22] The slight increase in
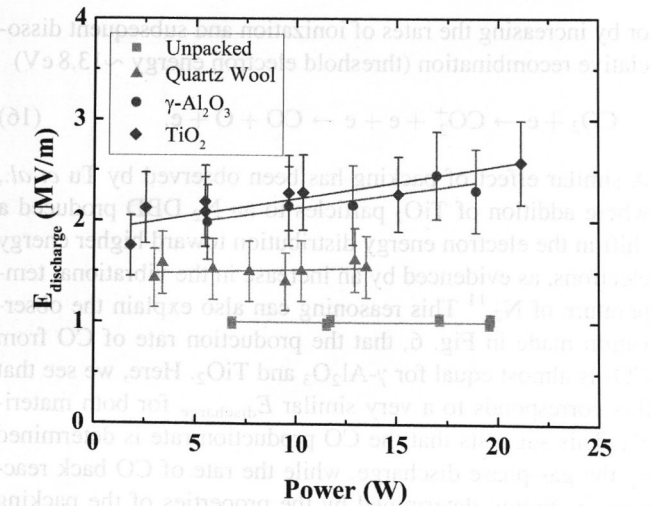

FIG. 11. (Color online) Maximum E-field found in the gas gap of the four configurations as a function of dissipated power. The lines are guides to the eye.

$E_{discharge}$ with power for γ-Al_2O_3 and TiO_2 can be argued to be due to highly inhomogeneous geometry of the gas gaps produced by the packing. With higher powers and higher applied voltages, larger areas are made to discharge, corresponding to $\beta = 0.2$ at the lowest depicted power for TiO_2 to $\beta = 1.0$ at the highest power in Fig. 11. This factor 5 increase in the maximum discharged area will necessarily correspond to more "unfavorable" locations being discharged, which correspond to higher breakdown fields and, hence, a higher average $E_{discharge}$ as power is increased.

Apart from the variation of $E_{discharge}$ as a function of power, the variation with packing material is of greater interest. In all cases $E_{discharge}$ is >1 MV/m, or >50 Td at atmospheric pressure. Filling the empty reactor with quartz wool increases the electric field required for discharging by a factor of ~1.5. For γ-Al_2O_3 and TiO_2 this is a factor of ~2.0 to 2.5. This can, qualitatively, be understood from the concept behind Meek's criterion for streamer formation: over shorter distances, a stronger electric field is required to achieve a certain minimal electron multiplication.[23] With packing, average gap widths are significantly smaller than the 3.8 mm of the empty reactor, and hence higher fields are required to ignite streamers in the DBD. This argument matches well with the differences between quartz wool, γ-Al_2O_3, and TiO_2 packing. Quartz wool packing leads to larger average gap widths in the reactor than γ-Al_2O_3 and TiO_2 packing, with the last two showing very similar $E_{discharge}$ because the packings are geometrically very similar.

There is also a clear correspondence between $E_{discharge}$ and CO_2 conversion. For example, adding quartz wool to the reactor, and thereby increasing $E_{discharge}$, translates directly into an increase in the average electron energy during discharging. While $E_{discharge}$ is too high to mainly stimulate vibrational excitation of CO_2,[24] an increase in electron energy can increase CO_2 conversion in the gas-phase simply by increasing the rate of dissociative attachment (threshold electron energy ~3.3 eV)

$$CO_2 + e \rightarrow CO_2^- \rightarrow CO + O^-, \tag{15}$$
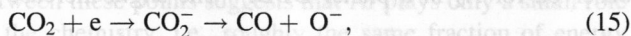
or by increasing the rates of ionization and subsequent dissociative recombination (threshold electron energy ~13.8 eV)

$$CO_2 + e \rightarrow CO_2^+ + e + e \rightarrow CO + O + e. \tag{16}$$
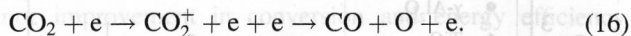
A similar effect of packing has been observed by Tu *et al.*, where addition of TiO_2 particles to an N_2 DBD produced a shift in the electron energy distribution toward higher energy electrons, as evidenced by an increase in the vibrational temperature of N_2.[11] This reasoning can also explain the observation made in Fig. 6, that the production rate of CO from CO_2 is almost equal for γ-Al_2O_3 and TiO_2. Here, we see that this corresponds to a very similar $E_{discharge}$ for both materials. This suggests that the CO production rate is determined by the gas-phase discharge, while the rate of CO back reactions is mainly determined by the properties of the packing surface. With the large scale geometry of both γ-Al_2O_3 and TiO_2 particles being very similar, it also appears likely that

the discharge is not strongly affected by the nature of the packing material, only by the geometry of the gas-filled voids it forms in the reactor. An important aspect in this regard could be the granular nature of the particles used here, which can be expected to possess many sharp edges leading to local E-field enhancement. The average field required for discharging $E_{discharge}$ obtained in this work may have been even higher if smoother particles of a similar size had been used.[17] Other work, however, has shown a direct relationship between dielectric constant of the packing and the conversion degree.[8,25] Ogata *et al.* observed a strong increase in benzene removal with increasing dielectric constant (using various mixed TiO_x-based materials) at constant specific energy input and pellet geometry.[25] On the other hand, for C_2F_6 removal using similar packing materials, no such dependence was observed.[26] How the dielectric constant of the packing material affects $E_{discharge}$ and the subsequent conversion degree is not an obvious relationship. A higher dielectric constant packing implies that more of the available applied voltage V is distributed over the gas gaps (and less over the packing) prior to discharging. To reach a certain $E_{discharge}$ (and achieve discharging) with a higher dielectric constant packing then simply requires a lower minimum applied voltage V, which would not immediately affect the properties of the discharge. The dielectric constant is, however, known to strongly affect the expansion of streamers, or microdischarges, on dielectric surfaces, occurring after ignition and propagation through the gas gap.[27] The relationship between dielectric constant and conversion efficiency could then be an indicator of the relevance of the surface expansion phase for the particular chemistry under study.

V. SUMMARY AND CONCLUSIONS

A cylindrical packed-bed DBD reactor has been studied using CO_2 and Ar gas mixtures with quartz wool, γ-Al_2O_3, and TiO_2 packing. The best performance is observed for TiO_2 packing in a 20% CO_2 in an argon mixture with 30% CO_2 conversion (at 2.9% energy efficiency), or alternatively a ~5.0% energy efficiency (at 17.5% CO_2 conversion). In terms of yield, at the highest efficiency, ~2 sccm of CO can be produced from 7 sccm of CO_2 using an input power of 15 W. The percentage of Ar in the flow has only a limited effect on conversion and energy efficiency. The conversion is a function of specific energy input, meaning the operation of the reactor does not change significantly whether power is increased or flow is decreased. Comparing results between γ-Al_2O_3 and TiO_2 packing using simplified kinetic models revealed that the production rate of CO is nearly equivalent for both packings (at ~0.1 s⁻¹ per CO_2 molecule), while the reverse reaction rates are two to three times lower for TiO_2 compared to γ-Al_2O_3. Electrical analysis of Q-V data revealed that the electric field at which breakdown occurs is also very similar for these two materials. Since the same particle sizes and void fractions are used for γ-Al_2O_3 and TiO_2, discharge behavior appears to be predominantly determined by geometry, not dielectric constant or surface properties.

From the preceding observations, it is suggested that the CO production rate is determined by the gas-phase discharge, while the rate of CO reverse reactions is mainly determined by the properties of the particle surfaces. This is consistent with the significantly higher BET surface area for γ-Al$_2$O$_3$ compared to TiO$_2$, so that the former can be expected to have increased rates for surface reactions between CO and oxygen species.

The electrical analysis applied in this work provides a quantitative assessment of discharge behavior in packed bed reactors which, combined with measured CO yields, provides a consistent picture of the contribution of packing to the conversion process. The conclusions drawn in this work could be tested further in a conventional plane-parallel reactor using γ-Al$_2$O$_3$ and TiO$_2$ as barriers, which can be more straightforwardly modeled than the complex geometry of a packed bed reactor. Dedicated experiments to determine the recombination rates between CO, O, or O$_2$ on these surfaces would also be beneficial to better understand the role of packing in the reactor.

ACKNOWLEDGMENTS

[1]B. Hu, C. Guild, and S. L. Suib, J. CO$_2$ Util. **1**, 18 (2013).
[2]A. Lebouvier, S. A. Iwarere, P. d'Argenlieu, D. Ramjugernath, and L. Fulcheri, Energy Fuels **27**, 2712 (2013).
[3]B. Ashford and X. Tu, Curr. Opin. Green Sustainable Chem. **3**, 45 (2017).
[4]A. Fridman, *Plasma Chemistry* (Cambridge University, Cambridge, England, 2008).
[5]E. C. Neyts and A. Bogaerts, J. Phys. D: Appl. Phys. **47**, 224010 (2014).
[6]D. Mei and X. Tu, Chem. Phys. Chem. **18**, 3253 (2017).
[7]X. Duan, Z. Hu, Y. Li, and B. Wang, AIChE J. **61**, 898 (2015).
[8]Q. Yu, M. Kong, T. Liu, T. J. Fei, and X. Zheng, Plasma Chem. Plasma Process. **32**, 153 (2012).
[9]D. Mei, D. X. Zhu, Y.-L. He, J. D. Yan, and X. Tu, Plasma Sources Sci. Technol. **24**, 015011 (2015).
[10]T. Butterworth, R. Elder, and R. Allen, Chem. Eng. J. **293**, 55 (2016).
[11]X. Tu, H. J. Gallon, and J. C. Whitehead, J. Phys. D: Appl. Phys. **44**, 482003 (2011).
[12]T. C. Manley, Trans. Electrochem. Soc. **84**, 83 (1943).
[13]F. J. J. Peeters and M. C. M. van de Sanden, Plasma Sources Sci. Technol. **24**, 015016 (2015).
[14]T. Butterworth and R. W. K. Allen, Plasma Sources Sci. Technol. **26**, 065008 (2017).
[15]N. den Harder *et al.*, Plasma Processes Polym. **14**, 1600120 (2017).
[16]K. Van Laer and A. Bogaerts, Energy Technol. **3**, 1038 (2015).
[17]I. Michielsen, Y. Uytdenhouwen, J. Pype, B. Michielsen, J. Mertens, F. Reniers, V. Meynen, and A. Bogaerts, Chem. Eng. J. **326**, 477 (2017).
[18]K. F. Young and H. P. R. Frederikse, J. Phys. Chem. Ref. Data **2**, 313 (1973).
[19]D. W. Green and R. H. Perry, *Perry's Chemical Engineer's Handbook*, 8th ed. (McGraw Hill, New York, 2008), pp. 2-7, 2-26.
[20]Y.-R. Zhang, K. Van Laer, E. C. Neyts, and A. Bogaerts, Appl. Catal. B **185**, 56 (2016).
[21]J. Kriegseis, B. Möller, S. Grundmann, and C. Tropea, J. Electrostat. **69**, 302 (2011).
[22]F. J. J. Peeters and M. C. M. van de Sanden, Plasma Sources Sci. Technol. **24**, 045006 (2015).
[23]C. Montijn and U. Ebert, J. Phys. D: Appl. Phys. **39**, 2979 (2006).
[24]A. Bogaerts, T. Kozák, K. Van Laer, and R. Snoeckx, Faraday Discuss. **183**, 217 (2015).
[25]A. Ogata, N. Shintani, K. Mizuno, S. Kishiyama, and T. Yamamoto, IEEE Trans. Ind. Appl. **35**, 753 (1999).
[26]K. Takaki, K. Urashima, and J.-S. Chang, IEEE Trans. Plasma Sci. **32**, 2175 (2004).
[27]V. I. Gibalov and G. J. Pietsch, J. Phys. D: Appl. Phys. **33**, 2618 (2000).